

Highly robust and hardware-efficient frame synchronization and carrier recovery via pilot-only approaches for short-reach optical interconnections

Chenchen Wang (王晨晨), Zhipei Li (李志沛)*, Ze Dong (董泽), Junyuan Song (宋俊元), Ran Gao (高然), Dong Guo (郭栋), Huan Chang (常欢), Lei Zhu (朱磊), Xiaolong Pan (潘晓龙), Tianle Mai (买天乐), Shanting Hu (胡善亭), and Xiangjun Xin (忻向军)

School of Information and Electronics, Beijing Institute of Technology, Beijing 100081, China

*Corresponding author: lizhipei@bit.edu.cn

Received November 12, 2024 | Accepted December 25, 2024 | Posted Online May 19, 2025

We propose a cost-effective scheme relying exclusively on pilot symbols for robust frame synchronization and high-precision, wide-range carrier recovery in short-reach optical interconnects. Our method mitigates phase offsets and enhances phase tracking by strategically placing dual-polarization pilot symbols, both aligned and misaligned, within the frame. Compared to traditional carrier recovery schemes, our approach offers a broader frequency offset estimation range, higher carrier recovery accuracy, and significantly lower computational complexity. Experimental results show a 0.7 dB sensitivity improvement at the soft decision forward error correction threshold, outperforming Fourier transform-based frequency offset estimation combined with blind phase search.

Keywords: frame synchronization; carrier recovery; pilot symbol; short-reach optical interconnect.

DOI: [10.3788/COL202523.060602](https://doi.org/10.3788/COL202523.060602)

1. Introduction

As network traffic in data centers (DCs) increasingly consists of internal server interactions, short-reach optical interconnections have become essential for information transmission^[1-3]. Optical transmission rates have progressed to 400 Gb/s, with expectations of reaching 800 Gb/s and even 1.6 Tb/s in the near future^[4]. Therefore, optical interconnections must deliver high transmission rates to meet growing data demands while ensuring cost-effectiveness and energy efficiency. The Optical Interconnect Forum (OIF) has developed frame structures for 400 Gb/s zebest range (ZR) scenarios^[5] that employ training sequences (TSs) for frame synchronization and initial frequency offset locking, utilizing pilot symbols for phase tracking. A well-known synchronization method is the Schmid algorithm^[6], which calculates correlation to identify the maximum value for precise timing. While this has inspired various enhanced synchronization schemes^[7,8], they often depend on specially designed TSs, limiting their flexibility. For the 800 Gb/s and 1.6 Tb/s long reach (LR) scenarios, however, the TS has been removed, and the interval between pilot symbols has increased from 32 to 64 symbols, as detailed in the OIF Implementation Agreement for the 800G LR scenario^[9]. This change necessitates the development of a new frame synchronization scheme, as it complicates synchronization and reduces the phase-tracking

capability of the pilot symbols. In addition, DCs demand high-speed data transmission at an affordable cost, necessitating the use of economical laser diodes. However, the affordability of these diodes often comes at the expense of accuracy, characterized by frequency fluctuations within the gigahertz range and wider linewidths. Therefore, a robust frame synchronization and optimal carrier recovery solution is urgently needed, ideally relying exclusively on pilot symbols.

In the absence of TSs and large interval pilot symbols, the conventional carrier recovery scheme is fast Fourier transform-based frequency offset estimation (FFT-FOE), combined with blind phase search (BPS)^[10-13]. Unfortunately, owing to the fourth power operation and the restricted FFT size, FFT-FOE has a limited estimation resolution and range [$\pm 1/2M$ symbol rate for M-ary phase shift keying (M-PSK) and $\pm 1/8$ symbol rate for M-ary quadrature amplitude modulation (M-QAM)]. Its high computational complexity further hinders its applicability in DCs, highlighting the need for innovative, cost-effective carrier recovery solutions. While pilot symbols can effectively facilitate FOE and carrier phase recovery (CPR)^[14], their effectiveness is influenced by pilot rates, which conflict with increasing information transmission demands. Notably, dual-polarized signals share identical carrier frequency offset (CFO) and laser phase noise (LPN), along with a constant phase offset^[15]. This opens up possibilities for pilot-aided polarization-joint carrier

recovery without additional overhead. In such a case, it is desirable to optimize the pilot position, the pilot symbol design, and the carrier recovery algorithm.

In this Letter, to meet the demand for low-cost, high-tolerance, and low-complexity digital signal processing (DSP) in short-reach optical interconnections, we design and optimize the position of pilot symbols and propose a cost-effective pilot-aided polarization-joint carrier recovery scheme. Our contributions are: (1) We propose a pilot-symbol-based synchronization scheme that employs constant phase intervals (PIs) between pilot symbols to tackle frame synchronization challenges in the absence of TSs. (2) We accurately estimate the constant phase offset between dual polarizations to facilitate polarization joint phase processing. With only a few pilot symbols, we achieve robust frame synchronization and subsequent carrier recovery, delivering exceptional performance. The estimation range can be expanded from $1/8N$ symbol rate (with a pilot rate of $1/N$) to $1/M$ symbol rate where M is the misalignment symbol interval. Experimental transmissions of 60-Gbaud dual-polarization 16-QAM (DP-16QAM) validate our scheme, showing a wide FOE range and enhanced precision. Moreover, our comparison of CPR capabilities for lasers with linewidths of 100 kHz and 1 MHz reveals that our scheme outperforms the FFT-FOE + BPS scheme, achieving a 0.7 dB improvement in receiving sensitivity at the soft decision forward error correction (SD-FEC) threshold.

2. Principle

The traditional methods of FOE using pilot symbols are affected by the fourth-power operation (removal of modulation information) and the pilot symbol interval. Additionally, increasing frame redundancy can expand the FOE range and enhance phase tracking capabilities. In this section, we provide a detailed explanation of achieving high-precision and stable frame synchronization using only pilot symbols. We also present a carrier recovery scheme based on polarization-joint pilot symbols. The proposed scheme does not suffer from the frame redundancy limitations and improves carrier recovery performance. Moreover, the proposed scheme demonstrates strong robustness against polarization mode dispersion (PMD), thereby ensuring high-performance carrier recovery.

2.1. Pilot-aided frame synchronization

For a coherent optical transmission system, the received signal contains CFO, LPN, and additive white Gaussian noise (AWGN) after clock recovery and multiple-input multiple-output (MIMO) equalization. Considering one sample per symbol, the pilot symbols received and processed by two polarizations at time k are described in the complex baseband as

$$\begin{cases} r_{x,k} = p_{x,k} e^{j\Delta\omega k + \theta_k} + n_{x,k} \\ r_{y,k} = p_{y,k} e^{j\Delta\omega k + \theta_k + \varphi} + n_{y,k} \end{cases}, \quad (1)$$

where $r_{x/y,k}$, $p_{x/y,k}$, and $n_{x/y,k}$ are the received symbols, transmitted symbols, and AWGN terms of X and Y polarizations.

$\Delta\omega = 2\pi\Delta f T_S$ is the angular frequency offset, where T_S is the symbol period. θ_k is the instantaneous phase of the LPN modeled as a Wiener process. φ is the phase offset of the two polarizations.

Through the time multiplexing of pilot symbols with payload symbols, the receiver can track the phase variations in real time. The pilot symbols formed from the outer symbols of 16QAM follow a quadrature phase-shift keying (QPSK) mapping with different X/Y polarization seeds^[9]. Frame synchronization using pilot symbols consists of two main steps: pilot extraction and the localization between the extracted pilot symbols and the transmitted pilot symbols. The extraction of pilot symbols uses both their insertion characteristics—where a pilot symbol is inserted at fixed intervals of N payload symbols—and their distribution properties. At the receiver side, we extract one symbol at every N interval from the received signal $r_{x/y,k}$, thereby obtaining N groups of symbols, each of length l . As shown in Fig. 1, among the extracted N groups of symbols [illustrated in Fig. 1(b) with $N = 64$ as an example], only the group containing pilot symbols exhibits the largest amplitude. The constellation diagram of the pilot symbols is depicted in Fig. 1(b). Consequently, we can obtain the indices of all pilot symbols. Frame synchronization is then determined by analyzing the variance of the PIs of the pilot symbols at corresponding positions in the two polarizations. The details are as follows:

It is apparent from Eq. (1) that $r_{x/y,k}$ depends on $p_{x/y,k}$. By multiplying the extracted pilot symbols conjugate to the transmitted pilot symbols, if the modulation information is correctly eliminated, let $z_{x/y,k} = r_{x/y,k} \cdot p_{x/y,k}^*$, we have

$$\begin{cases} z_{x,k} = e^{j\Delta\omega k + \theta_k} + n_{x,k}^* \\ z_{y,k} = e^{j\Delta\omega k + \theta_k + \varphi} + n_{y,k}^* \end{cases}, \quad (2)$$

where $n_{x/y,k}^*$ is the AWGN term included in the correlation operation. As shown in Fig. 2(a), the PIs between the pilot symbols of the same time slot in two polarizations, $\Delta\Phi_k$, are then obtained by

$$\Delta\Phi_k = \arg(z_{y,k+M} \cdot z_{x,k}^*) \approx \Delta n^* + \varphi. \quad (3)$$

Conversely, there is still the presence of modulation information difference in Eq. (3). Given that $\Delta n^* \approx 0$ and φ can be regarded as constant, in the case of frame synchronization, the PIs exhibit small fluctuations as shown in Fig. 2(b).

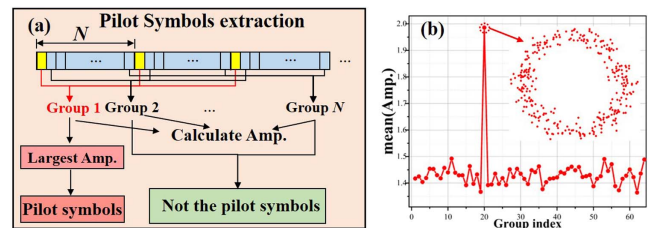


Fig. 1. (a) Schematic diagram of pilot symbol extraction; (b) mean amplitude of each group symbol.

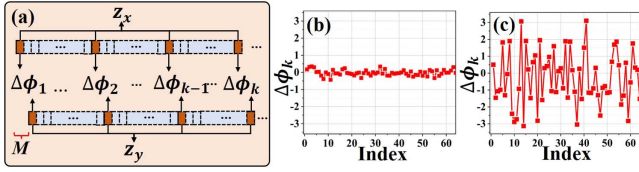


Fig. 2. Schematic diagram of pilot-aided frame synchronization. (a) Obtainment of the PIs between pilot symbols at the same time slot, and variation of PIs with (b) correct and (c) incorrect elimination of modulation information.

In contrast, Fig. 2(c) illustrates a scenario where pilot symbols are improperly positioned, leading to a substantial increase in PI fluctuation due to significant variations in modulation phase differences. To determine whether frame synchronization has been achieved, one can observe the variance of the PIs over a specified length. Considering L transmitted pilot symbols, we can slide the window to extract the next set of pilot symbols and repeat the process until synchronization is attained.

Frame synchronization using pilot symbols relies on the constant PIs between pilot symbols. This PI can be derived from pilot symbols placed on aligned polarizations in the same time slot, misaligned pilot symbols across polarizations, or pilot symbols on the same polarization separated by N symbol intervals (with a pilot rate of $1/N$). As such, the pilot-aided frame synchronization scheme is applicable to polarization-aligned frame structures, polarization-misaligned frame structures, and single-polarization scenarios.

2.2. Polarization-misaligned frame structure and polarization-joint pilot-aided FOE

As shown in Eq. (1), the phase information of the two polarizations can be processed jointly to enhance the carrier recovery performance. The idea is to insert pilot symbols in different time slots of the dual polarization.

Figure 3 illustrates the frame structure with polarization misalignment. Sec. I features dual-polarization aligned pilot symbols of length S , which are utilized for constant phase offset estimation. Sec. II is designed for pilot-aided frame synchronization and misaligned pilot-aided carrier recovery, with a length

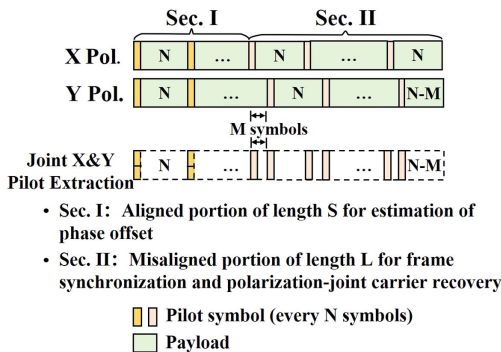


Fig. 3. Polarization misaligned frame structure.

of L . From Eq. (1), if the frame is synchronized, the modulation phase can be removed by multiplying $r_{x/y,k}$ by $p_{x/y,k}^*$ instead of $r_{x/y,k}^4$ because the fourth power operation will shorten the estimation range.

Figure 4 illustrates the block diagram of a pilot-aided frame synchronization and polarization-joint misaligned pilot-aided carrier recovery scheme that involves the initial FOE employing dual-polarization misaligned pilot symbols with an interval of M , the fine FOE utilizing single-polarization pilot symbols with an interval of N , the polarization-joint pilot-aided CPR, and a maximum likelihood (ML) estimator. $z_{x/y,k-s}^{1 \rightarrow S}$ and $z_{x/y,k}^{S+1 \rightarrow}$ in Fig. 4 represent the aligned and misaligned portions of the transmitted pilot symbols, where the superscript $1 \rightarrow S$ and $S+1 \rightarrow$ mean taking the S th pilot symbol from the first pilot symbol, and taking after the $S+1$ th pilot symbol.

In the frame structure shown in Fig. 3, the PIs between the misaligned pilot symbols of X polarization and Y polarization can be expressed as

$$\Delta\Phi_k = \arg(z_{y,k+M} \cdot z_{x,k}^*) \approx M \cdot \Delta\omega + \Delta\theta_M + \Delta n_M^* + \varphi. \quad (4)$$

It can be observed that PIs include CFO $M \cdot \Delta\omega$, phase noise difference $\Delta\theta_M$, and constant phase offset φ . Therefore, PIs not only serve as an indicator of frame synchronization but also are used for the initial stage of the polarization-joint coarse FOE after eliminating φ . We can estimate φ in the range of $(-\pi, \pi]$ from the pilot symbols of Sec. I. However, the $\arg(\cdot)$ function inherently returns values within the range of $(-\pi, \pi]$, which introduces a π phase ambiguity in the estimation process. To address the phase estimation ambiguity, φ needs to be adjusted to

$$\varphi = \frac{1}{S} \sum_{k=1}^S \arg(z_{y,k} \cdot z_{x,k}^*),$$

$$\varphi = \begin{cases} \varphi - 2\pi, & \varphi \geq \pi \\ \varphi + 2\pi, & \varphi \leq -\pi \end{cases}. \quad (5)$$

As shown in Fig. 4(a), we determine frame synchronization by evaluating the variance of PIs between the misaligned pilot symbols. The number of pilot symbols used for frame synchronization and the subsequent coarse FOE is L_1 . The PIs in Eq. (4), after subtracting φ , yield $M \cdot \Delta\omega + \Delta\theta + \Delta n^*$, which will be used for the first-stage polarization-joint coarse FOE, and obtain the coarse estimate of CFO Δf_{est1} ,

$$\Delta f_{est1} = \frac{1}{L_1} \sum_{L_1} (\Delta\Phi_k - \varphi). \quad (6)$$

We then employ pilot symbols of length L_2 for the second-stage fine estimation, preceded by rough compensation of the CFO using the first-stage estimation Δf_{est1} , as shown in Figs. 4(b) and 4(c). In coarse estimation, pilot symbols with dual-polarization misaligned M symbol intervals are utilized. Despite the wider estimation range afforded by this method,

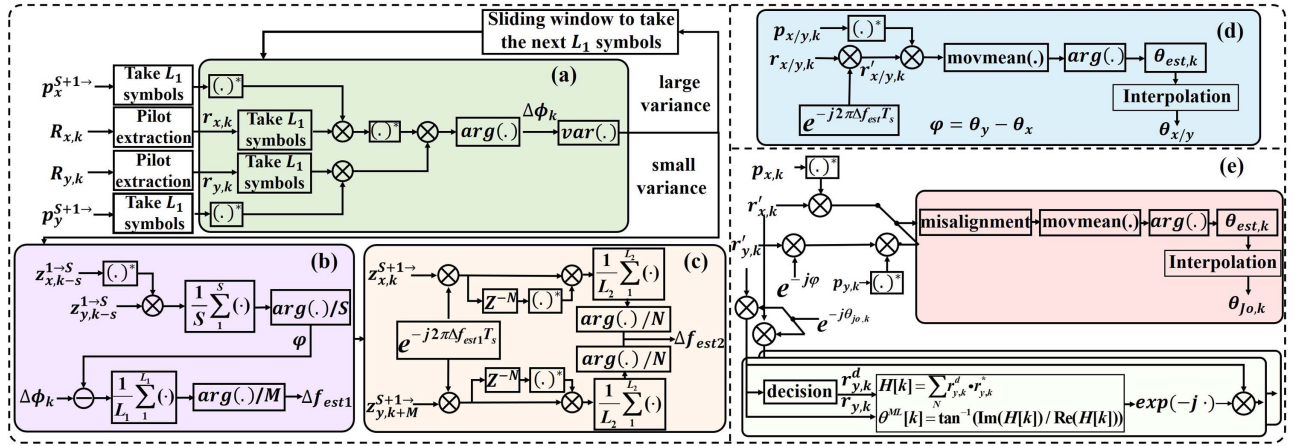


Fig. 4. Block diagram of the proposed polarization-joint misaligned pilot-aided carrier recovery scheme. (a) Pilot-aided frame synchronization; (b)–(c) two-stage cascade FOE; (d) phase offset fine estimation; and (e) pilot-aided CPR.

the presence of significant phase noise-induced PIs in Eq. (4) results in inaccuracies. Therefore, in the fine stage, pilot symbols with N symbol intervals are employed for enhanced accuracy. The final frequency offset is $\Delta f_{\text{est}} = \Delta f_{\text{est}1} + \Delta f_{\text{est}2}$, and the theoretical estimation can reach up to Eq. (7). When $M = 1$, the proposed approach theoretically enables a full FOE range of $\pm 1/2$ of the symbol rate,

$$-\frac{1}{M \times 2 \times T_s} \leq \Delta f_{\text{est}} \leq \frac{1}{M \times 2 \times T_s}. \quad (7)$$

According to Eq. (4), a smaller M increases the estimation range but also amplifies phase noise from sources other than CFO, reducing the accuracy of frequency offset calculations. As Eq. (4) also demonstrates, the presence of noise terms—particularly phase noise from the laser—poses challenges to accurate FOE computation. Larger phase noise diminishes the relative contribution of the CFO term, degrading FOE accuracy. However, our results indicate that the proposed method maintains both a wide estimation range and high accuracy, even under scenarios with significant laser phase noise.

After removing the CFO, phase noise estimation is conducted via the joint polarization extracted pilot symbols. Prior to this, the constant phase offset φ needs to be accurately compensated, as shown in Figs. 4(d) and 4(e). An accurate constant phase offset is obtained by subtracting P_L phase estimates of the respective polarizations from each other. Misaligned pilot symbols, containing only phase noise, are then extracted on the basis of the frame structure in Fig. 3 for subsequent polarization-joint phase estimation. A moving average filter is employed to mitigate the impact of AWGN. The polarization-joint estimation of the phase $\theta_{j_0,k}$ is then obtained by linearly interpolating over the time-division multiplexed pilot symbols extracted from the dual polarization. Finally, the residual phase noise is eliminated by a ML estimator.

2.3. Tolerance to PMD

The polarization-joint pilot-aided scheme relies on the joint processing of phase information from two polarization signals, making it essential to account for factors that may cause polarization phase disturbances. PMD is a key consideration. In short-reach coherent optical interconnections, PMD is typically small and can be compensated using the constant modulus algorithm (CMA). Although significant PMD can lead to mismatch between the frame structures of the received and transmitted signals, our algorithm maintains stable frame synchronization and provides high-precision, wide-range carrier recovery.

When PMD exceeds half of the symbol period, the misaligned symbol interval M transitions to M' ($M + 1$ or $M - 1$), leading to the PIs in Eq. (4), which turns into

$$\Delta \Phi_k = M' \cdot \Delta \omega + \Delta \theta_{M'} + \Delta n_{M'}^* + \varphi. \quad (8)$$

Frame synchronization can still be maintained through the principle of constant phase increment. The frame head of the Y polarization becomes $\text{id}_y - M' - N \times S$. The originally aligned pilot symbols at the front end become misaligned due to PMD, rendering them unsuitable for constant phase offset estimation. However, we can exploit the misalignment property of these pilot symbols to achieve precise FOE. When the PMD exceeds half of the symbol period, irrespective of which polarization resides on the fast axis, a coarse estimation of FOE can be derived by subtracting the PIs of the two portions of pilot symbols, obviating the need to estimate the constant phase offset between the two polarizations, as illustrated in Fig. 5. Similarly,

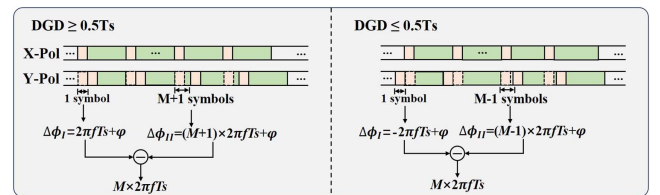


Fig. 5. Schematic diagram of FOE with large PMDs.

under these conditions, phase estimation can still be effectively carried out through interpolation using the pilot symbols extracted from joint polarization.

3. Numerical Simulation Demonstration

We conduct a simulation to evaluate the performance of the proposed scheme for an 800 Gb/s LR scenario. When $M = 1$, the complete FOE range of the $\pm 1/2$ symbol rate can theoretically be achieved. However, significant CFOs can render the CMA used for equalization ineffective, similar to heterodyne detection, especially considering that such significant CFOs are rare in practical scenarios. Consequently, our research focuses on $M = 2$, which also offers a sufficient estimation range. For validation, a DP-16QAM signal with a 123.6-Gbaud symbol rate, and a 64/63 pilot insertion ratio is used. In Fig. 3, $S = 20$, and the misaligned pilot symbol interval M can be adjusted arbitrarily to yield the corresponding estimation range, where M simultaneously influences both the FOE range and the CPR capability. Specifically, a larger M results in a smaller FOE range but allows for more accurate phase interpolation. The basic simulation conditions include a fiber length of 10 km and a linewidth of 1 MHz. In both simulations and experiments, the DSP algorithms and parameter configurations of the transmitter and receiver are consistent. Specifically, we utilize 20 pilot symbols for frame synchronization and coarse FOE estimation, followed by 120 symbols for fine FOE estimation.

We evaluate the estimation accuracy for different algorithms through Monte Carlo simulations, with the number of simulations set to 100. The estimation accuracies under different CFOs are explored separately for different values of M , as depicted in Fig. 6(a). In each Monte Carlo simulation, we set a certain CFO, and it varies randomly over a range of ± 50 MHz. The tracking ability under various CFOs is investigated and compared with the performance of the FFT-FOE algorithm in the above scenarios. The accuracy of the algorithm is expressed by the normalized estimation variance (MSE), which is defined as $E[(\Delta f - \Delta f_{est,n})T_s]^2$.

In the absence of frame synchronization, traditional pilot-aided FOE has a limited range of ± 0.2 GHz, which extends to only ± 0.8 GHz, even with the proposed synchronization method. In contrast, our new scheme significantly enhances

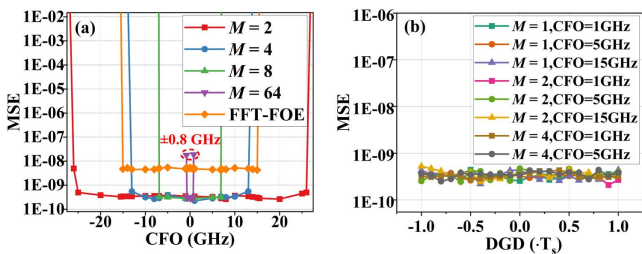


Fig. 6. (a) MSE curves with different CFOs for FFT-FOE, pilot-aided polarization-separate FOE ($M = 64$), and pilot-aided polarization-joint FOE ($M = 2, 4, 8$). (b) MSE versus DGD.

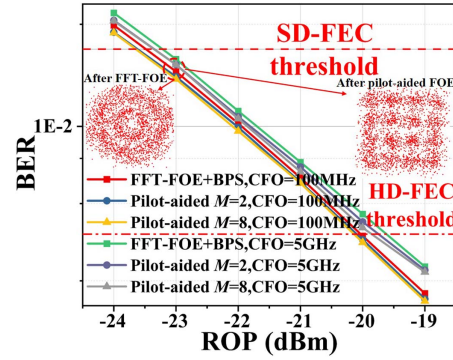


Fig. 7. BER versus optical signal-to-noise ratio (OSNR) for different carrier recovery schemes.

both estimation accuracy and range. Our findings also demonstrate its robustness against PMD, as shown in Fig. 6(b). We further validate the estimation performance under different differential group delays (DGDs) to demonstrate the tolerance of our proposed scheme to PMD. The CFO is set to 1, 10, and 15 GHz, with a ± 50 MHz random variation in Monte Carlo simulations. As can be seen from Fig. 6(b), our proposed scheme enables stable frame synchronization along with accurate and wide-range FOE, regardless of whether the misalignment interval M is 1 or greater, consistent with our previous analysis.

Ultimately, we analyzed the bit error rate (BER) performance of the proposed carrier recovery scheme in comparison to FFT-FOE+BPS. Figure 7 depicts the BER curves for both the classical FFT-FOE + BPS scheme and the pilot-aided carrier recovery scheme when $M = 2$ and 8. This evaluation considers CFOs at 100 MHz, with a linewidth of 1 MHz. The algorithms and parameters in the receiver side DSP are identical, except for the carrier recovery scheme. The constellation diagrams after frequency offset recovery using different schemes are shown in Fig. 7, where we conduct a comparison based on an arbitrary 5000 symbols located at the same position index. It can be observed that the signal contains almost no residual frequency offset after the pilot-aided polarization-joint FOE scheme, whereas the signal processed by the FFT-FOE exhibits a larger residual frequency offset. However, the FFT-FOE and the proposed scheme exhibit similar BER performance. This is attributed to the effectiveness of the BPS method in compensating for residual frequency offset. This aspect will be thoroughly analyzed in the experimental validation section. The simulation results show that the BER performance of the pilot-aided scheme surpasses that of the classical carrier recovery scheme while maintaining low computational complexity.

4. Experimental Verification and Discussion

4.1. Experimental setup

Figure 8 depicts the experimental block diagram. The offline DSP operation is implemented via MATLAB. At the transmitter, the pseudo-random binary sequences (PRBSs) of length 2^{15} are

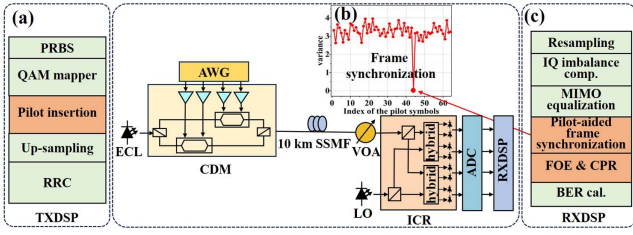


Fig. 8. Diagram of the experimental setup. RRC, root raised cosine; ECL, external cavity laser; SSMF, standard single-mode fiber; LO, local oscillator.

mapped as a 16QAM signal. The pilot sequence is inserted into both polarizations at a pilot rate of $1/64$, where the frame structure is shown in Fig. 3. The signal, after being twice upsampled, is injected into a 120-GSa/s sampling rate arbitrary waveform generator (AWG) with a 40 GHz 3-dB bandwidth and 8-bit resolution to generate 60 Gbaud signals. The electrical signals and continuous light waves are injected into the coherent driver modulator (CDM) for electro-optical conversion. The optical signal is then transmitted over distances of 10 km, with the received optical power (ROP) controlled by a variable optical attenuator (VOA). At the receiver side (Rx), the optical signal is received by an integrated coherent receiver (ICR). The detected electrical signals are captured by a 256 GSa/s analog-to-digital converter (ADC). The system bandwidth is around 40 GHz. The linewidths of the lasers used for performance evaluations are 100 kHz and 1 MHz. The block diagrams of the DSP employed at the Tx and Rx are illustrated in Fig. 8. Following resampling, in-phase and quadrature (IQ) imbalance compensation, and MIMO equalization, frame synchronization is performed via misaligned pilot symbols. As shown in Fig. 5(b), synchronization is achieved by analyzing the variance of PIs between the pilot symbols. Both FOE and CPR are implemented via the proposed scheme or FFT-FOE combined with BPS. Finally, signal demapping and BER counting are conducted to assess performance.

4.2. Assessment of BER gains achieved by the FOE algorithm

The simulation results demonstrate that our proposed scheme allows for the flexible selection of dual-polarization misalignment symbol intervals. Throughout the evaluation, the BPS algorithm was utilized for phase recovery. The signal length N_{sym} for FFT-FOE is set to 1024, with 32 test phases (B) for BPS, while the number of symbols per block N_b serves as the criterion for FOE accuracy. The numbers of pilot symbols used for FOE L_1 and L_2 are 20 and 120, respectively. Figures 9(a)–9(c)

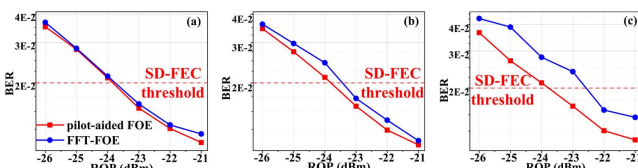


Fig. 9. BER curves versus ROP with $M = 2$ when $N_b =$ (a) 64, (b) 128, and (c) 256.

show the BER performance curves versus ROP with $M = 2$ when $N_b = 64, 128,$ and 256 . The BPS effectively compensates for the residual CFO, particularly at high symbol rates and small N_b . However, as N_b increases, BPS fails to compensate for the residual CFO resulting from FFT-FOE. In contrast, varying N_b yields no performance degradation within the proposed scheme, as the proposed scheme achieves highly accurate FOE with negligible residual frequency offset. Even at $N_b = 64$, the proposed FOE scheme has a 0.2 dB performance improvement over FFT-FOE near the threshold of $\text{BER} = 2.0 \times 10^{-2}$.

4.3. Assessment of BER gains achieved by the carrier recovery (FOE + CPR) algorithm

We first conducted experimental verification of the FOE range. Throughout the evaluation, either the proposed scheme or the combination of FFT-FOE and BPS is used for subsequent carrier recovery. Figure 10(a) illustrates the BER performance curves as a function of CFO for the proposed scheme and FFT-FOE + BPS, within their respective ranges, with a fixed ROP of -21 dBm; the BPS block size is 64. The BER performance curves reveal that the proposed scheme outperforms the FFT-FOE + BPS across the entire FOE range, extending up to ± 13 GHz compared to ± 7.5 GHz for FFT-FOE. This enhancement is attributed to the ability of the proposed scheme to overcome the limited resolution of the FFT-FOE and effectively utilize dual-polarization pilot symbols for carrier recovery. Even with significant CFO-induced signal spectrum distortion due to receiver bandwidth constraints [illustrated in Fig. 10(a)], the proposed scheme reliably computes the CFO. Figure 10(b) further demonstrates the superiority of the proposed scheme through improved constellation diagrams before and after CPR.

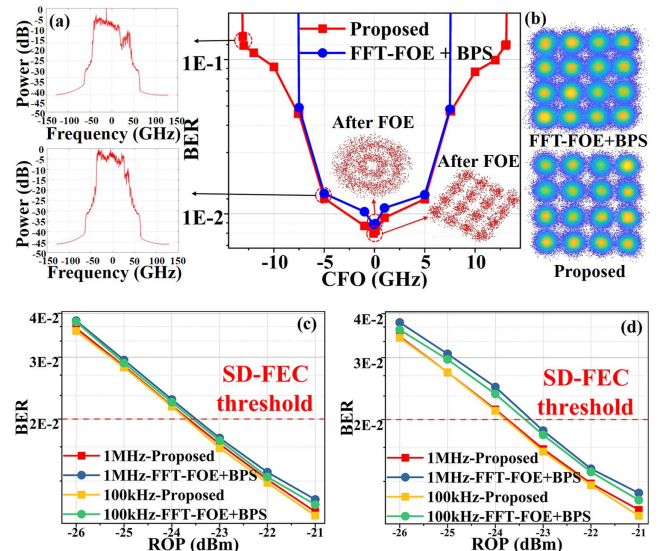


Fig. 10. (a) Spectrum under large CFOs; (b) constellation diagrams of different carrier recovery schemes. BER curves versus ROP when (c) $M = 2$ and (d) $M = 8$.

We finally evaluate the linewidth tolerance of the proposed scheme compared with that of FFT-FOE + BPS. Notably, with a laser linewidth of 1 MHz, the center frequency remains fixed, resulting in a CFO of approximately 2 GHz. To ensure a fair comparison, we set the CFO to 2 GHz for a linewidth of 100 kHz. Figures 10(c) and 10(d) show the BER curves for a 10 km transmission with varying linewidths, with M values of 2 and 8 at a 2 GHz CFO. The proposed scheme demonstrates ROP sensitivity improvements of approximately 0.3 and 0.7 dB over FFT-FOE + BPS at the SD-FEC threshold for $M = 2$ and 8, underscoring its potential for large-scale DC applications.

4.4. Computational complexity

We evaluate the computational complexity of the pilot-aided carrier recovery scheme and compare it with classical FFT-FOE + BPS. The number of real-valued multiplications and real-valued additions involved in the scheme is used as an indicator of the computational complexity of the DSP.

The complexity of the algorithm is shown in Table 1. $H = 10$ is the number of movmean filter taps. $P_L = 130$ is the number of phase estimates used to estimate φ accurately. When M is smaller, we need more pilot symbols since the PIs caused by the CFO account for a smaller portion. To reflect the complexity advantage of our scheme, we characterize the complexity of our scheme at $M = 2$ for all different M values when comparing the complexity. For the values of N_s , L_1 , and L_2 , we take $N_s = 1024$, $S = 20$, $L_1 = 20$, and $L_2 = 120$. All the above values are the boundary values when the estimated performance reaches the steady state. For BPS, we choose a phase value of $B = 32$ and a block size of $N_b = 64$. This selection ensures that BPS can compensate for residual frequency offset while maintaining stable performance in the FFT-FOE + BPS carrier recovery scheme.

Note that the computational complexity is assessed for dual polarization. Therefore, the complexities of BPS and

FFT-FOE need to be doubled. The computational complexity of the proposed frame synchronization method depends on the frame length. Using the 800 Gb/s LR frame structure recommended by OIF (96×64)^[9] and a misaligned pilot symbol length $L = 96 - 20 = 76$. In the worst-case scenario, frame synchronization requires $12L_1$ real multipliers and $6L_1$ real adders. Estimating constant phase offset for aligned symbols needs $12S$ real multipliers and $8S - 2$ real adders. To obtain the precise frequency estimation, the pilot-aided FOE scheme requires $24L_2$ real multipliers and $2L_1 + 16L_2 - 4$ real adders (including coarse frequency offset compensation for dual-polarization signals). The computational complexity for pilot-aided polarization separate CPR and joint CPR is the same, but individual polarization CPR requires two interpolations, while joint CPR requires three, due to the need for separate phase noise estimation and subtraction for each polarization. In light of these considerations, the complexity of the algorithm is shown in Table 1. The pilot-aided polarization-joint carrier recover scheme requires only 5.08% of the number of multiplications required for FFT-FOE + BPS, and only 4.15% of the number of additions.

5. Conclusion

We have proposed a cost-effective scheme for frame synchronization and carrier recovery solely utilizing pilot symbols for simplifying coherent DSP. Utilizing the principle of constant PIs between the pilot symbols enables frame synchronization. Following this, employing the pilot-aided polarization-joint carrier recovery scheme makes full use of the pilot symbols to achieve a wide estimation range and high-precision frequency estimation. Simulation results show that the scheme has a wider estimation range and more accurate estimation than FFT-FOE + BPS. Experiments with 10 km transmission over 60 Gbaud DP-16QAM verify that the proposed scheme can estimate the CFO up to ± 13 GHz despite severe band-limiting at the receiver side, and exhibits better BER performance, providing a 0.7 dB improvement in receiver sensitivity. The proposed scheme facilitates the realization of full-time-domain DSP architecture at the receiver side of the short-reach coherent optical interconnection in DCs, and represents a promising scheme for long-reach optical transmission systems.

Acknowledgements

This work was supported by the National Key R&D Program of China (No. 2022YFB2903103) and the National Natural Science Foundation of China (No. 62205023).

References

1. L. Zhu, H. Yao, H. Chang, *et al.*, "Adaptive optics for orbital angular momentum-based internet of underwater things applications," *IEEE Internet Things J.* **9**, 24281 (2022).
2. H. Wang, J. Zhou, Z. Xing, *et al.*, "Fast-convergence digital signal processing for coherent PON using digital SCM," *J. Lightwave Technol.* **41**, 4635 (2023).

Table 1. Computational Complexity.

	Multiplication	Addition
FFT-FOE	$16 N_s + 4 N_s \log_2 (N_s)$ 57344	$8 N_s + 4 N_s \log_2 N_s$ 49152
BPS	$6 N_b B + 4 N_b$ 12544	$5 N_b B + 2 N_b$ 10368
Pilot-aided frame synchronization	$12 L_1$ 240	$6 L_1$ 120
Pilot-aided FOE	$24 L_2$ 2880	$2 L_1 + 16 L_2 - 4$ 1956
Pilot-aided CPR	$3 N_b P + 7 N_b$ 451	$P_L + N_b (H - 1)/N + 4 N_b$ 395

3. K. Zhong, X. Zhou, J. Huo, *et al.*, "Digital signal processing for short-reach optical communications: a review of current technologies and future trends," *J. Lightwave Technol.* **36**, 377 (2018).
4. IEEE P802.3df 200 Gb/s, 400 Gb/s, 800 Gb/s, and 1.6 Tb/s ethernet task force (2023). <https://www.ieee802.org/3/df/public/index.html>.
5. OIF 400ZR (2019), <http://www.oiforum.com/technical-work/hot-topics/400zr-2/>.
6. T. M. Schmidl and D. C. Cox, "Robust frequency and timing synchronization for OFDM," *IEEE Trans. Commun.* **45**, 1613 (1997).
7. L. S. Gordon, *Principles of Mobile Communication* (Springer, 2017).
8. Z. Zhao, A. Yang, P. Guo, *et al.*, "Low-complexity frequency domain frame synchronization for short-reach IM/DD optical fiber transmission systems," *Opt. Express* **32**, 21077 (2024).
9. <https://www.oiforum.com/bin/c5i?mid=4&rid=7&gid=0&k1=53548&k2=3&k3=9>.
10. M. Selmi, Y. Jaouen, and P. Ciblat, "Accurate digital frequency offset estimator for coherent PolMux QAM transmission systems," in *2009 35th European Conference on Optical Communication* (2009), p. 1.
11. M. S. Faruk and S. J. Savory, "Digital signal processing for coherent transceivers employing multilevel formats," *J. Lightwave Technol.* **35**, 1125 (2017).
12. Y. Wang, E. Serpedin, P. Ciblat, *et al.*, "Non-data aided feedforward cyclostationary statistics-based carrier frequency offset estimators for linear modulations," in *GLOBECOM'01. IEEE Global Telecommunications Conference (Cat. No. 01CH37270)* (2001), p. 1386.
13. T. Pfau, S. Hoffmann, and R. Noé, "Hardware-efficient coherent digital receiver concept with feedforward carrier recovery for M-QAM constellations," *J. Lightwave Technol.* **27**, 989 (2009).
14. G. Li, A. Yan, S. Xing, *et al.*, "Pilot-aided continuous digital signal processing for multi-format flexible coherent TDM-PON in downstream," in *2023 Optical Fiber Communications Conference and Exhibition (OFC)* (2023), p. 1.
15. J. Lu, X. Li, S. Fu, *et al.*, "Joint carrier phase and frequency-offset estimation with parallel implementation for dual-polarization coherent receiver," *Opt. Express* **25**, 5217 (2017).